Published in final edited form as:
J Biomed Opt. 2009 ; 14(1): 014009. doi:10.1117/1.3065544.

Fluorescence Spectroscopy of Oral Tissue: Monte Carlo Modeling with Site-Specific Tissue Properties

Ina Pavlova[1], **Crystal Redden Weber**[2], **Richard A. Schwarz**[3], **Michelle D. Williams**[4], **Ann M. Gillenwater**[5], and **Rebecca Richards-Kortum**[3]

[1] Department of Biomedical Engineering, The University of Texas at Austin, Austin, Texas 78712

[2] Department of Chemistry, Rice University, Houston, Texas 77005

[3] Department of Bioengineering, Rice University, Houston, Texas 77005

[4] Department of Pathology, The University of Texas M.D. Anderson Cancer Center, Houston, Texas 77030

[5] Department of Head and Neck Surgery, The University of Texas M.D. Anderson Cancer Center, Houston, Texas 77030

Abstract

A Monte Carlo model with site-specific input was used to predict depth-resolved fluorescence spectra from individual normal, inflammatory, and neoplastic oral sites. Our goal in developing this model was to provide a computational tool to study how the morphological characteristics of the tissue affect clinically measured spectra. Tissue samples from the measured sites were imaged using fluorescence confocal microscopy; autofluorescence patterns were measured as a function of depth and tissue sublayer for each individual site. These fluorescence distributions were used as input to the Monte Carlo model to generate predictions of fluorescence spectra, which were compared to clinically measured spectra on a site-by-site basis. A lower fluorescence intensity and longer peak emission wavelength observed in clinical spectra from dysplastic and cancerous sites were found to be associated with a decrease in measured fluorescence originating from the stroma or deeper fibrous regions, and an increase in the measured fraction of photons originating from the epithelium or superficial tissue layers. The simulation approach described here can be used to suggest an optical probe design that samples fluorescence at a depth that gives optimal separation in the spectral signal measured for benign, dysplastic and cancerous oral mucosa.

Keywords

Spectroscopy; fluorescence spectroscopy; biomedical optics; tissues

1. Introduction

A number of small clinical studies have shown that fluorescence spectroscopy can diagnose oral neoplasia with sensitivity and specificity in the range 80–100% (1–5). Clinical data indicate that neoplastic progression in the oral cavity is associated with a number of characteristic spectral changes, including a drop in fluorescence intensity and a shift in peak fluorescence emission to longer wavelengths. These trends are thought to be caused by a series

Corresponding Author: Rebecca Richards-Kortum, Department of Bioengineering MS142, Rice University, 6100 Main St, Keck Hall Suite 116, Houston, Texas 77005, Phone: 713-348-5869, Fax: 713-348-5877, rkortum@rice.edu.

of physiological changes which accompany neoplastic progression in oral mucosa, such as increased light scattering and metabolic activity of cells throughout the epithelium, angiogenesis, and the remodeling of the stromal matrix.

While the pilot studies reported in (1–5) show promise, two factors are believed to limit the performance of spectroscopic algorithms for detection of oral neoplasia. First, the fluorescence properties of keratinized and non-keratinized anatomic sites in the oral mucosa differ substantially (6). Diagnostic algorithms must therefore account for variations in the degree of epithelial keratinization; different algorithms may be required to identify precancerous lesions arising in different anatomic sites such as the keratinized gingiva and the non-keratinized buccal mucosa. Second, the spectra of lesions with benign inflammatory changes can mimic those of oral premalignant lesions, reducing diagnostic specificity (7). A recent study used high-resolution autofluorescence confocal microscopy of fresh oral biopsies to investigate the biological basis for optical spectroscopy as a diagnostic aid for oral neoplasia and to help devise strategies to address these limitations (6). Precancerous tissues showed a loss of stromal autofluorescence and increased epithelial cell fluorescence compared to normal tissue; in contrast, lesions with chronic inflammation showed epithelial fluorescence similar to normal tissue, but exhibited a similar loss of stromal autofluorescence as lesions diagnosed with dysplasia (6). Thus, optical spectroscopy devices which separately record signals from the epithelium and stroma may improve the ability to distinguish benign inflammation from dysplasia.

Improving the accuracy of fluorescence spectroscopy requires a detailed understanding of how changes in the morphology and biochemistry of a specific oral tissue site affect measured autofluorescence spectra. This understanding must include variations that occur with anatomic location, benign inflammation, and neoplasia. Monte Carlo modeling of light propagation in tissue can be an important tool to investigate the relationship between the optical properties of tissue and the resulting fluorescence emission spectrum.

Monte Carlo based models have been used to study light propagation in multilayered tissue to investigate the effect of changes in optical properties on predicted spectra in several organ sites (8–11). We designed a Monte Carlo model to predict fluorescence spectra of normal and neoplastic oral mucosa; this model incorporated a three dimensional distribution of fluorescent sources determined by high-resolution fluorescence microscopy (12). We used this model to predict depth-resolved fluorescence spectra from normal and dysplastic oral mucosa (12). The model was validated by simulating average normal and dysplastic fluorescence spectra and comparing the predictions to average clinical data. Spectra of neoplastic tissue predicted using Monte Carlo analysis had a lower intensity and a longer peak emission wavelength than those predicted for normal oral mucosa; these predictions are consistent with changes observed in the average spectra measured from normal and neoplastic oral mucosa.

However, sensitivity analysis of Monte Carlo predictions suggests that results of the depth-sensitive Monte Carlo model are sensitive to changes in the optical properties of the epithelium and the superficial stroma (12). Small changes in the total epithelial thickness, epithelial keratinization, and fluorescence intensity of the superficial stroma can lead to significant changes in the shape and intensity of predicted spectra. Thus, while Monte Carlo predictions of spectra of normal and neoplastic oral tissue agree with average clinical data, it has been difficult to assess whether Monte Carlo models can accurately predict the spectrum of a particular tissue site given information about the three-dimensional distribution of chromophores within that particular tissue.

The goal of this study was to evaluate the ability of a Monte Carlo model with site-specific input properties to predict individual depth-resolved spectra from normal, inflammatory, and

neoplastic oral mucosa. Fluorescence spectra were measured *in vivo* from clinically normal and abnormal sites in the oral mucosa. Measured sites were biopsied, and high resolution fluorescence confocal microscopy was used to record the autofluorescence patterns as a function of depth at each individual site. These fluorescence distributions were used as input to the Monte Carlo model to predict tissue fluorescence spectra at each individual site. Predicted spectra were compared to measured spectra on a site-by-site basis.

The results of the Monte Carlo model were used to elucidate possible biological reasons for variations in clinical depth-resolved spectra measured from normal, inflammatory, and neoplastic oral tissue. We show that developing an accurate modeling approach to predict site-specific fluorescence spectra could improve our understanding of how morphological and biochemical changes associated with specific benign, precancerous and cancerous conditions influence the shape and intensity of clinically measured spectra. While validation of this model requires input obtained from biopsy, once validated, the model can be used to aid in designing optical instrumentation and diagnostic algorithms to non-invasively distinguish among spectra measured from benign, dysplastic and cancerous sites.

2. Methods

2.1 Overview

The study was reviewed and approved by the Institutional Review Boards at the University of Texas at Austin, the University of Texas M.D. Anderson Cancer Center, and Rice University. Fluorescence spectra were measured *in vivo* from clinically normal and abnormal oral sites using a fiber optic probe which preferentially collects fluorescent light generated in the epithelium and superficial stroma. Biopsies were obtained from measured sites, and high resolution fluorescence confocal microscopy was used to record autofluorescence patterns as a function of depth at each site. Using these site-specific fluorescence distributions as input to a Monte Carlo model, we predicted the tissue fluorescence spectrum for each site. Predicted fluorescence spectra for six oral sites with different pathological diagnoses and/or anatomical types were compared to the clinical spectra measured at each site.

2.2 Depth-sensitive Monte Carlo modeling of oral mucosa

A fixed weight Monte Carlo program was used to simulate the collection of fluorescence spectra using a fiber optic probe designed to preferentially collect fluorescence generated in the epithelium and superficial stroma. The program was designed to account for generation and propagation of fluorescent light in multilayered oral tissue. Details regarding the Monte Carlo code and the depth-sensitive fiber optic probe geometry have been described previously (12). Briefly, excitation photons were initially propagated through the tissue using the scattering coefficient (μ_s) and absorption coefficient (μ_a) at the excitation wavelength according to the layer they are traveling through. A photon has a probability of $\mu_a/(\mu_s+\mu_a)$ being absorbed at a scattering site. If a photon is absorbed by a fluorophore an emission photon may be generated and is propagated according to the μ_a and μ_s for the emission wavelength in the layer in which it is traveling. The photons are propagated until they reach the surface or are reabsorbed. The number of photons that reach the surface and are detected by a detector are calculated. A single simulation output predicts the fluorescence emission at 350 nm excitation, and consists of the detected fluorescence intensity (total number of detected fluorescence photons) at emission wavelengths of 400 nm, 420 nm, 440 nm, 450 nm, 460 nm, 480 nm, 500 nm, 520 nm, 540 nm and 560 nm. Each simulation was performed with 10^8 excitation photons. For each detected photon, the depth at which fluorescence emission occurred was recorded. The fraction of detected photons originating in the epithelium and the fraction originating in the stroma were calculated.

2.3 Clinical measurements, biopsy collection and high resolution tissue imaging

Fluorescence emission spectra at 350 nm excitation were measured from clinically normal and abnormal sites using a depth-sensitive fiber optic probe. Detailed descriptions of the clinical spectroscopic device, the depth-sensitive fiber optic probe, and procedures for patient recruitment, data acquisition, calibration, and processing have been reported in (5). The optical probe contains four depth channels, each consisting of a set of illumination and collection fibers arranged in a geometric configuration designed to preferentially collect light from a specific depth region in the tissue. The shallow channel, which was used to collect the clinical data presented here, uses a ball lens at the tip of the probe to redirect the angle of the illumination light such that its intersection with the collection region is localized to the tissue surface; this enables preferential collection of signal from the epithelium and superficial stroma.

Data from six sites in three patients were used to validate the Monte Carlo model. To explore variations in spectroscopic data with the presence of benign inflammation and neoplasia, data were selected from a patient with measurements made from four sites in the tongue with histologic diagnoses of normal, inflammation, dysplasia and cancer. To explore variations with tissue anatomic site, measurements were selected from two additional patients with measurements of normal palate and normal buccal mucosa. After spectroscopic measurement, each site was biopsied and the tissue sample was divided into two portions. One portion of each sample was sent for histologic examination. Transverse 200 micron thick tissue slices were immediately prepared from the second portion of each sample and imaged with a confocal fluorescence microscopy while the tissue was still viable. Confocal images were obtained at ultraviolet (UV; 350 nm and 364 nm) excitation and at 488 nm excitation to determine input parameters to the Monte Carlo model for that site. Detailed procedures for tissue preparation, confocal imaging and quantitative analysis of autofluorescence patterns are described in (6).

2.4 Tissue geometry and model input parameters

For normal, inflammatory, and dysplastic sites, tissue was modeled as a multilayered turbid medium with five sublayers: superficial epithelium, intermediate epithelium, basal epithelium, superficial stroma, and deep stroma (6,12). Each sublayer was assumed to contain a single dominant fluorophore, characteristic of that sublayer and diagnosis. At each site, the UV confocal fluorescence images were analyzed to determine the thickness and average fluorescence intensity of each sublayer; these values were used as site-specific input to the Monte Carlo model.

Previous work has shown that the superficial epithelium includes cells that retain keratin, and the main fluorophore in this layer was assumed to be keratin (6). The primary fluorophore in the intermediate epithelium was assumed to be mitochondrial flavin adenine dinucleotide (FAD) (6). The dominant fluorophore in the basal epithelium was assumed to be mitochondrial reduced nicotinamide adenine dinucleotide (NADH) (6). For the normal and dysplastic sites, the primary fluorophores in both the superficial and deep stroma were assumed to be collagen crosslinks (13). In oral lesions with severe stromal inflammation, confocal microscopy studies demonstrate stromal fluorescence that appears to originate from inflammatory cells with strong cytoplasmic fluorescence at UV excitation. Thus for the inflammatory site considered in this study, the dominant stromal fluorophore was assumed to be mitochondrial NADH.

The site diagnosed as invasive cancer was modeled using a different tissue geometry, because the normal structure is lost with invasion. This site was modeled as a turbid medium with cellular and fibrous layers; the geometry was derived from visual examination of the confocal images obtained from the measured site. Five sublayers were defined: cellular region 1, with dominant keratin fluorescence and optical properties similar to non-cancerous superficial epithelium; cellular region 2, with weak cytoplasmic fluorescence from FAD; cellular region

3, with bright cytoplasmic fluorescence from NADH; matrix region 1, with dominant NADH fluorescence associated with a significant cellular component consisting of cancer, inflammatory, and atypical cells; and matrix region 2, a fibrous region with collagen as the primary fluorophore and optical properties similar to those of non-cancerous deep stroma.

The scattering coefficients of the epithelial and stromal layers were obtained from previous studies of oral, cervical and bronchial tissue. The values of the scattering coefficients at 350 nm and absorption coefficients at 420 nm are summarized in Table 1. The scattering coefficient of the intermediate and basal epithelium was derived from reflectance confocal images of normal, dysplastic and cancerous non-keratinized oral epithelium (14). The scattering coefficient of the superficial epithelium in all oral sites considered in this study was derived from reflectance confocal measurements of cervical keratinized epithelium (15). In normal oral tissue the scattering coefficients for the superficial and deep stromal layers were assumed to be the same and were based on values from (16). To accurately model the drop in stromal scattering associated with oral dysplasia, the scattering coefficient in the superficial stroma in the dysplastic case was decreased by 20% (17). Scattering coefficients obtained from the literature were extrapolated to lower wavelengths using the inverse proportionality relationship of cellular scattering to wavelength (18).

The absorption coefficient for the epithelium was assumed to be constant for all sites considered in this study and was based on values derived in (16). The stromal absorption coefficient used in this model has contributions from three different absorbers: collagen, oxy-hemoglobin, and deoxy-hemoglobin. The collagen absorption coefficient was based on measurements from bloodless skin samples (19). The oxy- and deoxy-hemoglobin absorption coefficients were calculated as described by Jacques et al (20). An oxygen saturation level of 80% and a hemoglobin concentration of 150 g/l were used.

For the normal tongue site and the dysplastic tongue site, the volume fraction of blood in the stroma was determined from quantitative analysis of images from hematoxylin and eosin (H&E) stained slides from that specific site. H&E images of these sites were analyzed to estimate the fraction of the total stromal area occupied by blood. The estimated value included areas occupied by the lumen of blood vessels. The volume fraction of blood in the superficial stromal layer of the normal tongue site was estimated to be in the range 0.05–0.1%, while the value for deep stroma was in the range 0.2–0.3%. The superficial stromal layer underlying the epithelium in the dysplastic tongue site was estimated to have a volume fraction of blood in the range 0.10–0.20%, while the value for deep stroma was similar to that of the normal case. The values obtained for the normal tongue site were used for the other normal sites as well. For the cancer site and the inflammatory site, the volume fraction of blood in the stroma was estimated based on information from the literature. For the cancer site, the volume fraction of blood was estimated as 4 times higher than that of normal tissue, based on previous research indicating that the microvessel density of oral cancers is about 3–4 times higher than in normal oral tissue (21). For the inflammatory site, the volume fraction of blood was estimated to be similar to the blood volume fraction of normal tissue.

3. Results

3.1 Site-specific spectral changes caused by neoplastic progression in oral mucosa

Figure 1 shows confocal fluorescence images and measured clinical spectra obtained at UV excitation from four different sites on the tongue of a single patient. One of the four sites was clinically and histologically normal; the other three sites were oral lesions that were diagnosed histologically as inflammation, dysplasia, and cancer, respectively. The normal oral tissue is characterized by strong epithelial and stromal autofluorescence (Fig. 1a). In contrast, the oral lesion diagnosed with severe inflammation displays a large drop in both epithelial and stromal

fluorescence (Fig. 1b). In addition, while stromal fluorescence in the normal tissue originates from collagen fibers, fluorescence from the inflammatory stroma originates predominantly from a large influx of inflammatory cells. The oral lesion diagnosed with dysplasia is characterized by increased epithelial thickness, brightly fluorescent cells throughout the epithelium, and a drop in fluorescence of the superficial stroma (Fig. 1c). Confocal images of a malignant lesion diagnosed with moderately differentiated cancer (Figure 1d) illustrate the loss of layered architecture typical for cancers. In this example the superficial 400 microns of the tissue are occupied by cancer cells; underneath is a region of matrix infiltrated by cancer cells and inflammatory cells.

Clinically measured emission spectra at 350 nm excitation from the four oral sites are displayed in Fig. 1e. The data illustrate the characteristic drop in overall intensity associated with neoplastic progression in oral mucosa. Spectra from the dysplastic and cancerous sites also have lower relative emission intensity in the 400–430 nm wavelength region, giving them a different spectral shape compared to the normal case. The spectrum from the inflammatory site displays both a drop in fluorescence intensity and a shift to a longer peak emission wavelength compared to the normal spectrum.

Table 2 summarizes the site-specific tissue properties that were derived from confocal fluorescence images of each site. At a given site, each of the five tissue sublayers was assigned a thickness, a dominant fluorophore, and a relative fluorescence intensity based on quantitative analysis of the confocal fluorescence images.

Depth-resolved spectra for all tissue sites were simulated with the Monte Carlo based model at 350 nm excitation using the input values shown in Tables 1 and 2. Figure 2 compares the predicted spectra to the clinically measured spectra of the four tongue sites. The simulated spectra accurately predict the drop in fluorescence intensity and changes in spectral shape displayed in this example of neoplastic progression in oral mucosa (Fig. 2a–d).

The fraction of photons originating from the epithelium and the fraction originating from the stroma were calculated for each simulation (Fig. 2e–h). In the normal case (Fig. 2e), the detected fluorescence includes both a significant epithelial and stromal component. For example, at 450 nm the fraction of photons originating from the epithelium is approximately equal to the fraction of photons originating from the stroma, and the stromal contribution dominates the total fluorescence in the 400–420 nm region. With the presence of inflammation (Fig. 2f), the fraction of photons originating from the stroma substantially drops, while the fraction of epithelial photons increases. It should be noted that the decreased fraction of stromal photons is due to a large reduction in fluorescence originating from the stroma and not due to an increase in fluorescence originating from the epithelium. Thus the overall intensity of the predicted spectrum from the inflammation site is very low compared to the simulations from normal tissue. In the dysplastic tissue sample (Fig. 2g), the fraction of photons originating from the epithelium is very high for all emission wavelengths. Here, the high fraction of epithelial photons is due to a very large reduction of stromal fluorescence and a significant increase of epithelial fluorescence compared to the normal case. As a result, the overall fluorescence intensity of the simulated dysplastic spectrum is lower than the normal case but not as low as in the inflammation case. Thus, while both the dysplastic and inflammatory lesions show a drop in stromal fluorescence, the overall fluorescence intensity and fraction of epithelial photons of the dysplastic tissue is greater than that of the inflammatory tissue due to the increase in fluorescence originating from the dysplastic epithelium. In the cancerous tissue case (Fig. 2h), the fraction of fluorescence from the deep fibrous region is extremely low, and the overall fluorescence intensity is low as well. This is due to sharply reduced fluorescence from the deeper matrix region and slightly reduced fluorescence from the upper cellular regions of the cancer lesion relative to the analogous regions in normal tissue.

3.2 Site-specific spectral changes caused by variations in keratinization

Figure 3 shows high resolution confocal images of normal oral mucosa taken from two different anatomic sites that display different epithelial fluorescence patterns. The normal buccal site (Fig. 3a) is characterized by a weakly fluorescent superficial layer, while the normal palate site (Fig. 3b) displays a brightly fluorescent superficial epithelium. Clinical fluorescence spectra at 350 nm excitation measured from both sites are displayed in Fig. 3c.

Figure 4 compares the Monte Carlo predictions to the clinically measured spectra of the normal buccal mucosa and normal palate sites. The fluorescence spectrum of the palate site has greater intensity and is blue shifted relative to the spectrum measured from the buccal site; these trends are accurately predicted by the model (Fig. 4a–b). Predictions for the buccal mucosa site are within 10% of the measured spectra. However, the predicted intensity of the palate site is lower than that measured *in vivo*, possibly due to experimental error in estimating the thickness of the superficial epithelial layer. Previous model sensitivity analysis performed with the depth-sensitive Monte Carlo model has shown that even variations of 50 microns in the thickness of the superficial layer can result in a noticeable effect on the total intensity of the prediction (12). The estimated thickness of the strongly fluorescent keratin layer from the confocal images has a large standard deviation, which could explain the difference in intensity between the simulated and clinical spectra.

Figure 4 also summarizes the fraction of photons originating from the epithelium and the stroma derived from depth analysis of the simulated spectra. The buccal mucosa has a large fraction of photons originating from the stroma (Fig. 4c), compared to the palate site (Fig. 4d). Here, the larger fraction of epithelial photons can be attributed mainly to increased fluorescence from the epithelial layer of the palate site. Additional analysis (data not shown) indicates that the increased epithelial fluorescence originates from the superficial, keratinized region of the epithelium in the palate site. We suggest that the presence of a brightly fluorescent keratin layer in the palate site increases the fluorescence originating from the superficial epithelium compared to the buccal site, which accounts for the higher intensity of the palate spectrum compared to the buccal spectrum. The increased contribution from keratin also affects the spectral shape of the fluorescence from the palate site; the measured spectrum of the palate site shows similarities to the emission spectrum of keratin, which displays a peak at 420 nm.

4. Discussion

Our results demonstrate that a Monte Carlo modeling approach with site-specific tissue parameters measured using confocal fluorescence microscopy can predict variations in clinically measured fluorescence spectra of oral tissue. Further, the model shows how specific morphological and biochemical differences among anatomic sites and disease states can affect the fluorescence signal.

The output of Monte Carlo based models is dependent on the input parameters and geometry used to represent the tissue of interest. Multilayered Monte Carlo models tend to have a large number of input parameters and may produce similar output with different sets of parameters. Some of these predictions, while agreeing well with clinical data, could be physiologically unrealistic. The use of experimentally derived, site specific input parameters can improve the biological validity of the Monte Carlo based predictions. The approach described in this study enables the prediction of spectra using optical characteristics specific for the tissue site of interest, rather than using general tissue properties for a given anatomic site and disease status. This brings the model closer to representing the actual tissue that produced the measured spectra. In addition it allows for a more accurate analysis of the relationship between alterations in optical properties of a specific oral lesion and the fluorescence spectra measured from that lesion. This approach is useful primarily for exploring the origins of autofluorescence in normal

and abnormal tissue; it depends, of course, on the availability of a tissue sample from the measured site.

The site-specific Monte Carlo model accurately predicted the general trends in fluorescence intensity and spectral shape observed in the clinical data from the six sites analyzed in this study (Figs. 2 and 4). Agreement between the predicted and measured spectra was closest for the non-keratinized oral sites with layered morphology: the normal and dysplastic tongue sites and the normal buccal mucosa. The prediction was slightly less accurate for the keratinized site (normal palate) and for the lesions diagnosed with inflammation and cancer. Determination of accurate tissue geometry from confocal images is more difficult for cases with large local differences in morphology, such as the cancer lesion, or in cases with variations in the thickness of a strongly fluorescent superficial epithelium, such as the palate site. Thus, spectra from keratinized or cancerous sites may be more challenging to predict accurately using this model than spectra from non-keratinized sites with layered morphology.

In this study, variations were observed in the spectra measured from normal tissue at different anatomic sites. Analysis of the site-specific predictions shows that the origins of the detected autofluorescence are different in the non-keratinized and keratinized sites. For the non-keratinized normal sites (buccal mucosa and tongue), the measured signal was attributed to a combination of stromal fluorescence and epithelial fluorescence. For the keratinized normal site (palate), the blue shift and increase in overall fluorescence intensity were attributed to a significant increase in the contribution of photons originating from the superficial keratinized layer to the total detected signal.

These observations are consistent with reports in the literature that superficial epithelium in oral mucosa can vary significantly in the degree of keratinization depending on the anatomic site, and that these variations significantly affect autofluorescence spectra. Muller et al. reported differences in fluorescence spectra measured *in vivo* from keratinized and non-keratinized oral mucosa (2), related to a reduction in the depth of penetration of excitation light due to scattering from the keratin layer. De Veld et al. reported that the different degree of keratinization displayed by oral lesions is a factor that complicates accurate differentiation of benign from malignant oral lesions using autofluorescence spectroscopy (7).

The site-specific predictions of the normal, dysplastic and cancerous fluorescence spectra displayed a decrease in fluorescence intensity and a shift to longer peak emission wavelength with neoplastic progression. Analysis of the origin of predicted fluorescence indicated that the lower fluorescence intensity seen in the dysplastic and cancerous spectra was due predominantly to a decreased fluorescence originating from the stroma or deeper fibrous regions, whereas the spectral red shift was attributed to an increase in the fraction of photons originating from the epithelium or superficial cellular layers. These results were similar to those obtained in a previous study, in which the depth-dependent Monte Carlo model was used to predict average normal and dysplastic oral fluorescence spectra (12). In addition, results from a mathematical model analysis for extracting the intrinsic fluorescence spectra from *in vivo* fluorescence spectra from the oral cavity and the cervix (2,22) confirm that malignant progression is characterized by an increase in the epithelial contribution and a decrease in the stromal contribution to the total detected fluorescence.

The Monte Carlo simulations of spectra from the inflammatory site and the cancer site are of particular interest, since inflammation can be a confounding factor in spectroscopic diagnosis of neoplasia. As shown in Fig. 2, the intensity and spectral shape of the measured fluorescence spectra are quite similar for the inflammatory site and the cancer site. However, the origin of the signal is different in the two cases. The fluorescence signals from both the inflammatory and cancer sites are characterized by low stromal fluorescence and moderately low epithelial

fluorescence relative to normal tissue. The cancer site, however, displays a more pronounced drop in stromal fluorescence compared to the inflammation site. In addition, the contribution from the cellular regions is higher in the cancer site than the epithelial contribution in the inflammatory site. Thus, while the total predicted fluorescence from the cancer site is dominated by epithelial photons, the spectrum from the inflammatory lesion has a significant stromal component. While these results are specific for a particular example of neoplastic progression in the oral tongue, they suggest that depth-sensitive spectroscopy, with further improvements in depth resolution and instrumentation to fully isolate the signal originating from the epithelium and/or stroma, may provide a potentially useful method to distinguish inflammation from neoplasia.

In addition to using the model to suggest an optimal depth to improve differentiation between inflammation and cancer, similar analysis can be done to improve differentiation between the varying degrees of dysplasia and cancer. Another important application for this model is determining whether different anatomical sites can be grouped together for diagnosis or whether inherent differences such as keratinization cause the spectra to differ enough that the classification is compromised. The model can address this by studying the spectral effect caused by a keratin layer of varying thickness compared to the changes cause by neoplastic progression. If there is a depth at which the spectral signature of the neoplastic progression is independent of the keratin layer then a device which measures at that depth would not be sensitive to the anatomical site keratinization.

The results of this study indicate that a Monte Carlo model with site-specific input parameters extracted from confocal images can accurately predict depth-resolved fluorescence spectra from individual oral sites. The model provides information regarding the origin of detected photons within different tissue sublayers. This information may be useful in designing strategies to improve the ability of optical spectroscopy to accurately distinguish among normal, benign and malignant oral sites.

Acknowledgments

The authors thank Dr. Adel K. El-Naggar for providing pathology diagnoses, and Bimal Patel and Erica M. Smith for performing clinical measurements. The authors gratefully acknowledge support from National Institutes of Health grant R01 CA095604.

References

1. Heintzelman DL, Utzinger U, Fuchs H, Zuluaga A, Gossage K, Gillenwater AM, Jacob R, Kemp B, Richards-Kortum RR. Optimal excitation wavelengths for *in vivo* detection of oral neoplasia using fluorescence spectroscopy. Photochem Photobiol 2000;72(1):103–113. [PubMed: 10911734]
2. Muller MG, Valdez TA, Georgakoudi I, Backman V, Fuentes C, Kabani S, Laver N, Wang Z, Boone CW, Dasari RR, Shapshay SM, Feld MS. Spectroscopic detection and evaluation of morphologic and biochemical changes in early human oral carcinoma. Cancer 2003;97:1681–1692. [PubMed: 12655525]
3. de Veld DCG, Skurichina M, Witjes MJH, Duin RPW, Sterenborg HJCM, Roodenburg JLN. Autofluorescence and diffuse reflectance spectroscopy for oral oncology. Lasers Surg Med 2005;36:356–364. [PubMed: 15856507]
4. Wang CY, Tsai T, Chen HM, Chen CT, Chiang CP. PLS-ANN based classification model for oral submucous fibrosis and oral carcinogenesis. Lasers Surg Med 2003;32:318–326. [PubMed: 12696101]
5. Schwarz RA, Gao W, Daye D, Williams MD, Richards-Kortum R, Gillenwater AM. Autofluorescence and diffuse reflectance spectroscopy of oral epithelial tissue using a depth-sensitive fiber-optic probe. Appl Opt 2008;47(6):825–834. [PubMed: 18288232]

6. Pavlova I, Williams M, El-Naggar A, Richards-Kortum R, Gillenwater A. Understanding the biological basis of autofluorescence imaging for oral cancer detection: High-resolution fluorescence microscopy in viable tissue. Clin Cancer Res 2008;14:2396–2404. [PubMed: 18413830]
7. de Veld DCG, Skurichina M, Witjes MJH, Duin RPW, Sterenborg HJCM, Roodenburg JLN. Clinical study for classification of benign, dysplastic, and malignant oral lesions using autofluorescence spectroscopy. J Biomed Opt 2004;9(5):940–950. [PubMed: 15447015]
8. Chang SK, Marin N, Follen M, Richards-Kortum R. Model-based analysis of clinical fluorescence spectroscopy for *in vivo* detection of cervical intraepithelial dysplasia. J Biomed Opt 2006;11(2): 024008. [PubMed: 16674198]
9. Arifler D, MacAulay C, Follen M, Richards-Kortum R. Spatially resolved reflectance spectroscopy for diagnosis of cervical precancer: Monte Carlo modeling and comparison to clinical measurements. J Biomed Opt 2006;11(6):064027. [PubMed: 17212550]
10. Qu J, MacAulay C, Lam S, Palcic B. Laser-induced fluorescence spectroscopy at endoscopy: tissue optics, Monte Carlo modeling, and *in vivo* measurements. Opt Eng 1995;34(11):3334–3343.
11. Hidovic-Rowe D, Claridge E. Modelling and validation of spectral reflectance for the colon. Phys Med Biol 2005;50:1071–1093. [PubMed: 15798309]
12. Pavlova I, Weber CR, Schwarz RA, Williams M, El-Naggar A, Gillenwater A, Richards-Kortum R. Monte Carlo model to describe depth selective fluorescence spectra of epithelial tissue: Applications for diagnosis of oral precancer. J Biomed Opt 2008;13:064012. [PubMed: 19123659]
13. Sokolov K, Galvan J, Myakov A, Lacy A, Lotan R, Richards-Kortum R. Realistic three-dimensional epithelial tissue phantoms for biomedical optics. J Biomed Opt 2002;7(1):148–156. [PubMed: 11818022]
14. Clark AL, Gillenwater A, Alizadeh-Naderi R, El-Naggar AK, Richards-Kortum R. Detection and diagnosis of oral neoplasia with an optical coherence microscope. J Biomed Opt 2004;9(6):1271–1280. [PubMed: 15568948]
15. Collier T, Follen M, Malpica A, Richards-Kortum R. Sources of scattering in cervical tissue: determination of the scattering coefficient by confocal microscopy. Appl Opt 2005;44(11):2072–2081. [PubMed: 15835356]
16. Qu J, MacAulay C, Lam S, Palcic B. Optical properties of normal and carcinomatous bronchial tissue. Appl Opt 1994;33(31):7397–7405.
17. Arifler D, Pavlova I, Gillenwater A, Richards-Kortum R. Light scattering from collagen fiber networks: micro-optical properties of normal and neoplastic stroma. Biophys J 2007;92:3260–3274. [PubMed: 17307834]
18. Mourant JR, Freyer JP, Hielscher AH, Eick AA, Shen D, Johnson TM. Mechanisms of light scattering from biological cells relevant to noninvasive optical-tissue diagnostics. Appl Opt 1998;37(16):3586–3593. [PubMed: 18273328]
19. Saidi, IS. PhD Dissertation. Rice University; Houston, TX: 1992. Transcutaneous optical measurement of hyperbilirubinemia in neonates.
20. Jacques, SL. Skin optics. Oregon Medical Laser Center News. 1998 . http://omlc.ogi.edu/news/jan98/skinoptics.html
21. Macluskey M, Chandrachud LM, Pazouki S, Green M, Chisholm DM, Ogden GR, Schor SL, Schor AM. Apoptosis, proliferation, and angiogenesis in oral tissues. Possible relevance to tumour progression. J Pathol 2000;191:368–375. [PubMed: 10918211]
22. Georgakoudi I, Jacobson BC, Muller MG, Sheets EE, Badizadegan K, Carr-Locke DL, Crum CP, Boone CW, Dasari RR, Van Dam J, Feld MS. NAD(P)H and collagen as *in vivo* quantitative fluorescent biomarkers of epithelial precancerous changes. Cancer Res 2002;62:682–687. [PubMed: 11830520]

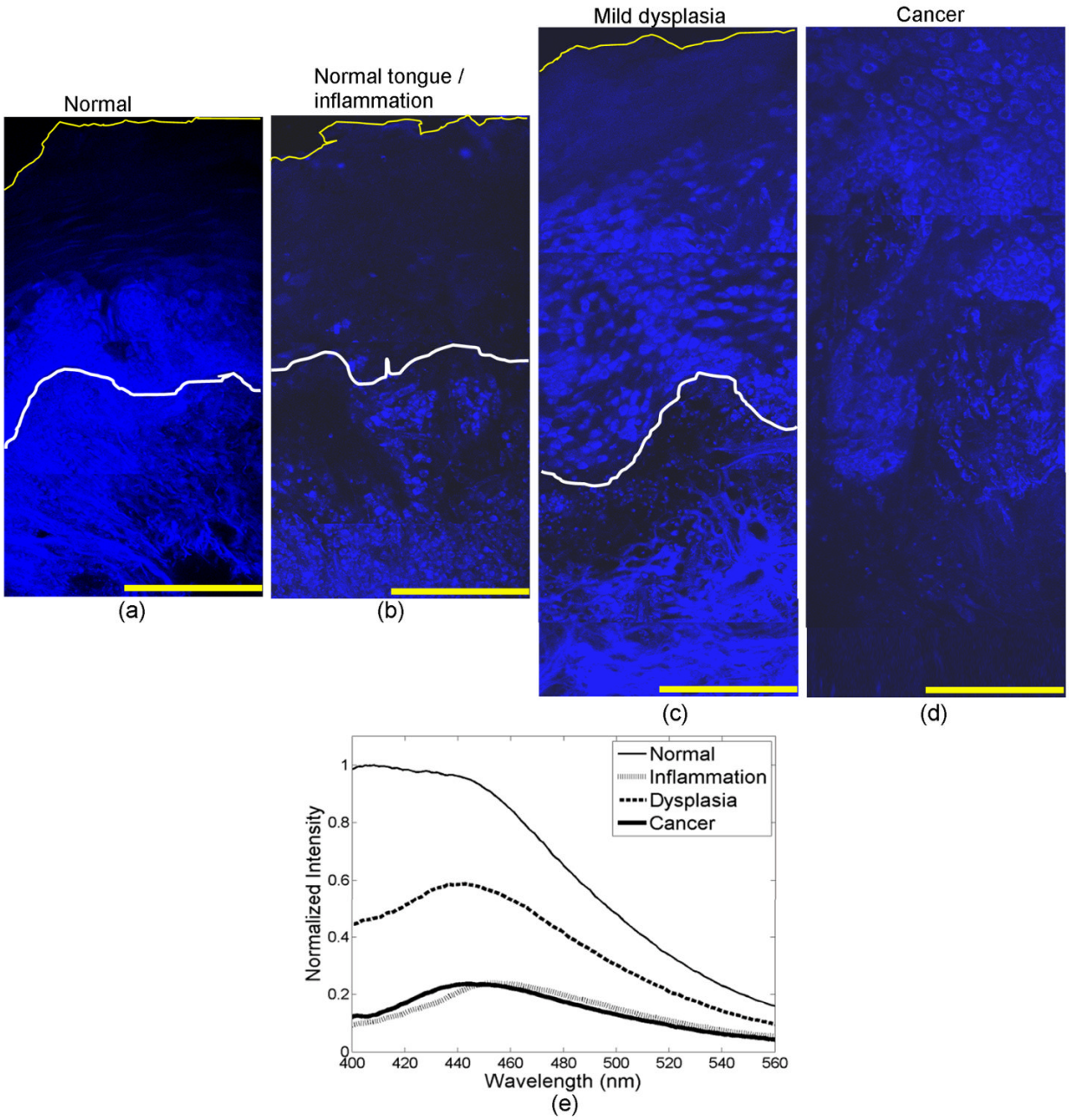

Figure 1.

(a–d) Fluorescence confocal images and (e) measured fluorescence spectra at UV excitation, showing neoplastic progression in the tongue. (a) Normal tongue; (b) normal tongue with severe stromal inflammation; (c) focal mild dysplasia; (d) moderately differentiated cancer. In (a–c), the white lines represent the basement membrane and the yellow lines represent the tissue surface. Scale bars represent 200 μm. (e) Fluorescence spectra at 350 nm excitation, measured from the same oral sites shown in the confocal images. Images (b, c) are reproduced from (6) with permission.

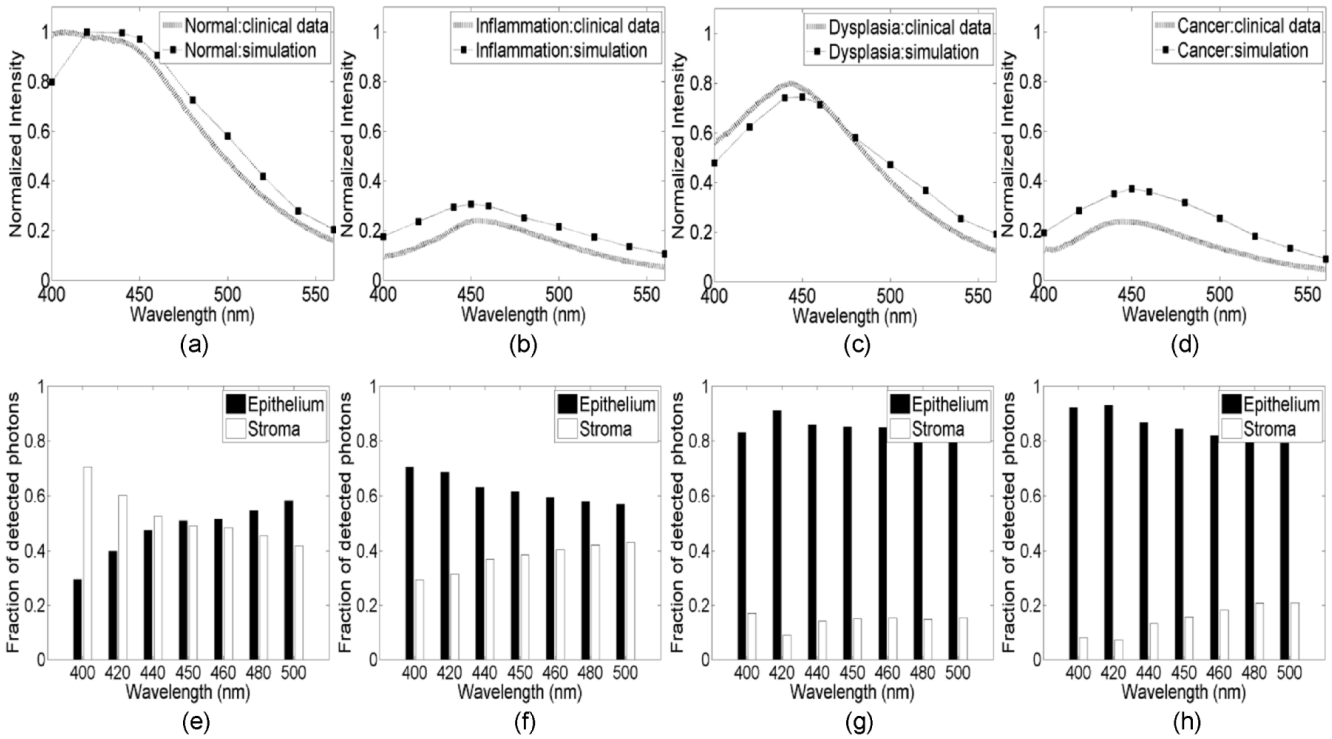

Figure 2.

Comparison of Monte Carlo model predictions with clinical fluorescence spectra measured from four oral tongue sites in the same patient. Clinical data and predictions at 350 nm excitation from (a) normal tongue, (b) normal tongue with severe inflammation, (c) focal mild dysplasia, and (d) moderately differentiated cancer. Bar graphs showing the predicted fraction of detected photons originating from the epithelium and the stroma for the (e) normal, (f) inflammatory and (g) dysplastic simulations. (h) Bar graph showing the predicted fraction of detected photons originating from the cellular region (upper 400 microns) and the deeper fibrous region for the cancer simulation.

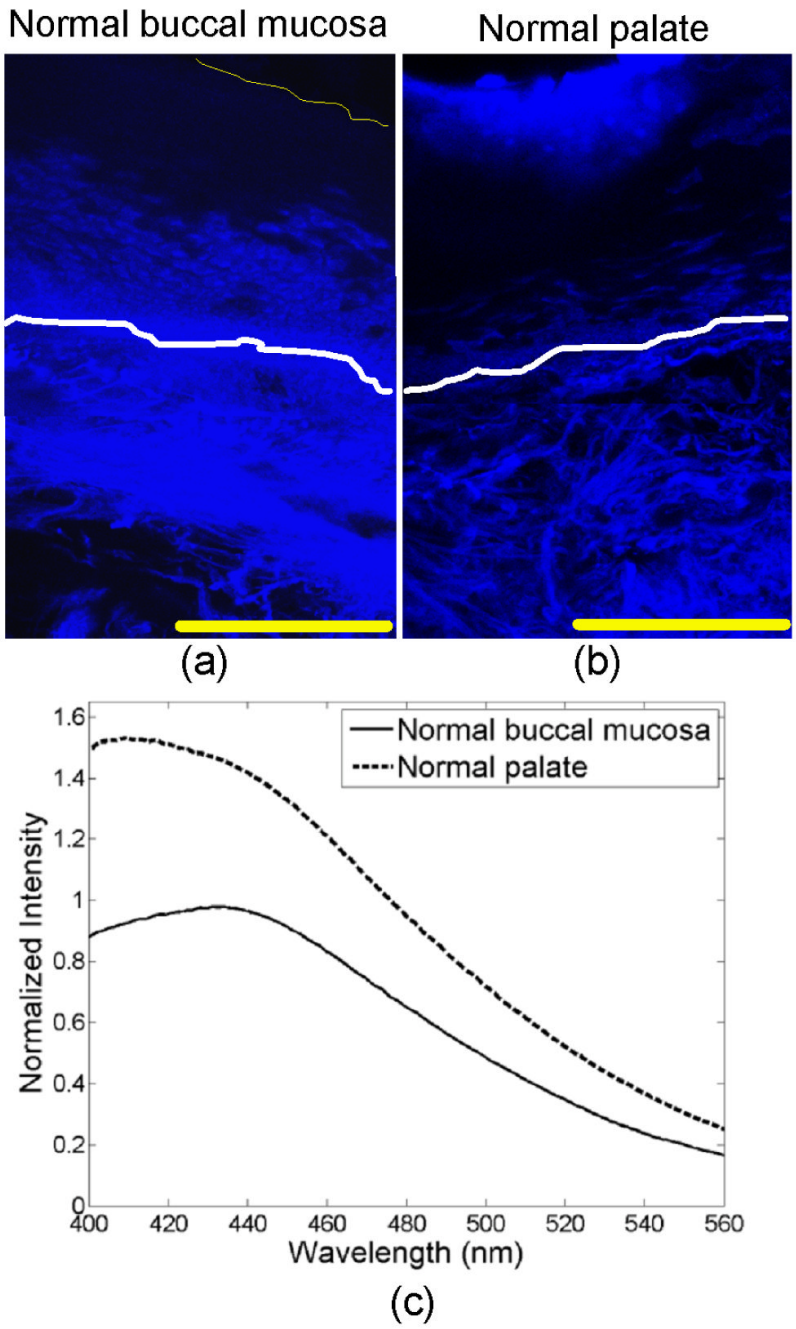

Figure 3.

(a–b) Fluorescence confocal images and (c) measured fluorescence spectra at UV excitation, showing changes in autofluorescence patterns due to anatomic site variation. (a) Normal buccal mucosa; (b) normal palate. In (a–b), the white lines represent the basement membrane and the yellow lines represent the tissue surface. Scale bars represent 200 μm. (c) Fluorescence spectra at 350 nm excitation, measured from the same oral sites shown in the confocal images.

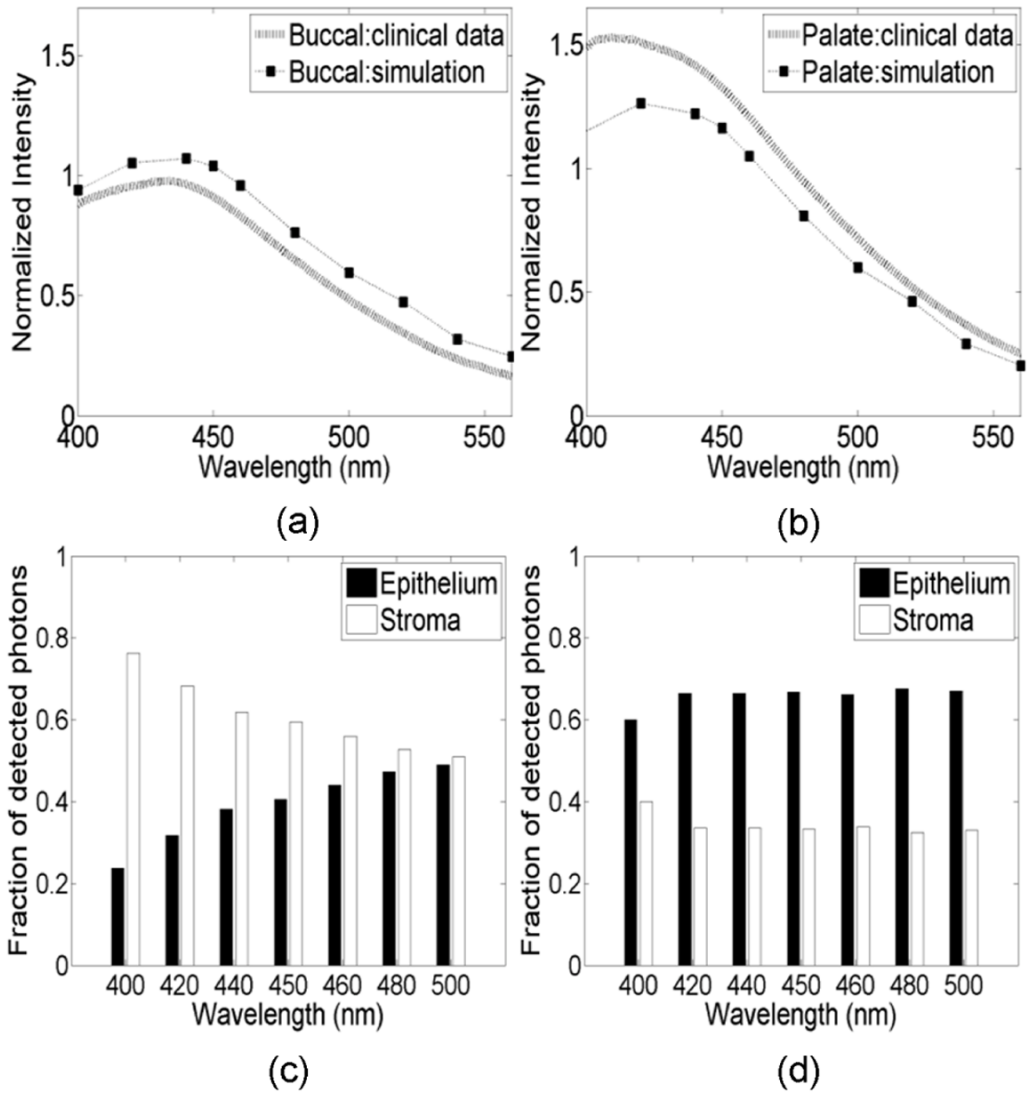

Figure 4.

Comparison of Monte Carlo model predictions with clinical fluorescence spectra measured at different anatomic sites in the oral cavity. Clinical data and predictions at 350 nm excitation from (a) normal buccal mucosa and (b) normal palate. Bar graphs showing the predicted fraction of detected photons originating from the epithelium and stroma for (c) normal buccal mucosa and (d) normal palate.

Table 1

Scattering and absorption coefficients for each oral tissue site and sublayer. Values were used as input to the Monte Carlo model.

	Normal Tongue	Severe Inflamm. (Tongue)	Mild Dysplasia (Tongue)	Normal Buccal Mucosa	Normal Palate		Cancer (Tongue)
Superficial Epithelium						Cellular Region 1	
μs (cm-1) at 350 nm	204	204	204	204	204	μs (cm-1) at 350 nm	204
μa (cm-1) at 420 nm	3	3	3	3	3	μa (cm-1) at 420 nm	3
Intermediate Epithelium						Cellular Region2	
μs (cm-1) at 350 nm	66	66	66	66	66	μs (cm-1) at 350 nm	66
μa (cm-1) at 420 nm	3	3	3	3	3	μa (cm-1) at 420 nm	3
Basal Epithelium						Cellular Region 3	
μs (cm-1) at 350 nm	66	66	95	66	66	μs (cm-1) at 350 nm	121
μa (cm-1) at 420 nm	3	3	3	3	3	μa (cm-1) at 420 nm	3
Superficial Stroma						Matrix Region 1	
μs (cm-1) at 350 nm	320	320	256	320	320	μs (cm-1) at 350 nm	160
μa (cm-1) at 420 nm	6.22	6.22	6.4	6.22	6.22	μa (cm-1) at 420 nm	21.5
Deep Stroma						Matrix Region 2	
μs (cm-1) at 350 nm	320	320	320	320	320	μs (cm-1) at 350 nm	160
μa (cm-1) at 420 nm	21.5	21.5	21.5	21.5	21.5	μa (cm-1) at 420 nm	21.5

Table 2

Thickness, dominant fluorophore, and relative fluorescence intensity for each oral tissue site and sublayer. Values were used as input to the Monte Carlo model.

	Normal Tongue	Severe Inflamm. (Tongue)	Mild Dysplasia (Tongue)	Normal Buccal Mucosa	Normal Palate		Cancer (Tongue)
Superficial Epithelium						Cellular Region 1	
Thickness (μm)	80	80	111	40	90	Thickness (μm)	95
Fluorophore	keratin	keratin	keratin	keratin	keratin	Fluorophore	keratin
Relative Intensity	0.12	0.12	0.3	0.12	0.9	Relative Intensity	0.11
Intermediate Epithelium						Cellular Region 2	
Thickness (μm)	80	120	70	100	90	Thickness (μm)	100
Fluorophore	FAD	FAD	FAD	FAD	FAD	Fluorophore	FAD
Relative Intensity	0.26	0.17	0.4	0.22	0.16	Relative Intensity	0.22
Basal Epithelium						Cellular Region 3	
Thickness (μm)	120	100	277	130	85	Thickness (μm)	200
Fluorophore	NADH	NADH	NADH	NADH	NADH	Fluorophore	NADH
Relative Intensity	0.8	0.15	0.8	0.74	0.35	Relative Intensity	0.4
Superficial Stroma						Matrix Region 1	
Thickness (μm)	125	125	125	125	125	Thickness (μm)	300
Fluorophore	collagen	NADH	collagen	collagen	collagen	Fluorophore	NADH
Relative Intensity	0.86	0.15	0.3	0.88	0.7	Relative Intensity	0.2
Deep Stroma						Matrix Region 2	
Thickness (μm)	20000	20000	20000	20000	20000	Thickness (μm)	20000
Fluorophore	collagen	NADH	collagen	collagen	collagen	Fluorophore	collagen
Relative Intensity	0.86	0.15	0.7	0.9	0.7	Relative Intensity	0.2